Noncollinear magnetic structure and anisotropic magnetoelastic coupling in cobalt pyrovanadate $Co_2V_2O_7$

W. H. Ji,[1] L. Yin,[2] W. M. Zhu,[3] C. M. N. Kumar,[4] C. Li,[5] H.-F. Li,[6] W. T. Jin,[7] S. Nandi,[1] X. Sun,[1] Y. Su,[7] Th. Brückel,[1] Y. Lee,[8] B. N. Harmon,[8] L. Ke,[8,*] Z. W. Ouyang,[2,†] and Y. Xiao[3,‡]

[1]*Jülich Centre for Neutron Science JCNS and Peter Grünberg Institut PGI, JARA-FIT, Forschungszentrum Jülich GmbH, 52425 Jülich, Germany*

[2]*Wuhan National High Magnetic Field Center, Huazhong University of Science and Technology, Wuhan 430074, China*

[3]*School of Advanced Materials, Peking University, Shenzhen Graduate School, Shenzhen 518055, China*

[4]*Institut für Festkörperphysik, TU Wien, Wiedner Hauptstrasse 8-10/138, 1040 Wien, Austria*

[5]*Jülich Centre for Neutron Science JCNS, Forschungszentrum Jülich GmbH, Outstation at SNS, P.O. Box 2008, 1 Bethel Valley Road, Oak Ridge, Tennessee 37831-6473, USA*

[6]*Joint Key Laboratory of the Ministry of Education, Institute of Applied Physics and Materials Engineering, University of Macau, Avenida da Universidade, Taipa, Macau SAR 999078, China*

[7]*Jülich Centre for Neutron Science JCNS at Heinz Maier-Leibnitz Zentrum, Forschungszentrum Jülich GmbH, Lichtenbergstraße 1, 85747 Garching, Germany*

[8]*Ames Laboratory, U.S. Department of Energy, Ames, Iowa 50011, USA*

(Received 27 June 2019; published 14 October 2019)

$Co_2V_2O_7$ was recently reported to exhibit remarkable magnetic-field-induced magnetization plateaus and ferroelectricity [R. Chen *et al.*, Phys. Rev. B **98**, 184404 (2018)], but its magnetic ground state remains ambiguous. Magnetometry measurements and time-of-flight neutron powder diffraction (NPD) have been employed to study the structural and magnetic properties of $Co_2V_2O_7$, which includes two nonequivalent Co sites. Upon cooling below the Néel temperature $T_N = 6.0(2)$ K, we observe magnetic Bragg peaks at 2 K in NPD, which indicates the formation of long-range magnetic order of Co^{2+} moments. After symmetry analysis and magnetic structure refinement, we demonstrate that $Co_2V_2O_7$ possesses a complicated noncollinear magnetic ground state with Co moments mainly located in the *b*-*c* plane and forming a noncollinear spin-chain-like structure along the *c*-axis. The *ab initio* calculations demonstrate that the noncollinear magnetic structure is more stable than various ferromagnetic states at low temperature. The noncollinear magnetic structure with a canted ↑↑↓↓ spin configuration is considered to be the origin of magnetoelectric coupling in $Co_2V_2O_7$ because the inequivalent exchange striction induced by the spin-exchange interaction between the neighboring spins could be the driving force of ferroelectricity. It is also found that the deviation of lattice parameters *a* and *b* is opposite below T_N, while the lattice parameter *c* and β stay almost constant below T_N, evidencing the anisotropic magnetoelastic coupling in $Co_2V_2O_7$.

DOI: 10.1103/PhysRevB.100.134420

I. INTRODUCTION

Low-dimensional spin systems have attracted extensive interest because their low dimensionality and complex multiple-spin exchange interactions often lead to novel ground states as well as intriguing magnetic behavior, such as spinon excitations in the one-dimensional (1D) spin-chain system $KCuF_3$ [1,2], and a spin liquid state in the two-dimensional (2D) triangular lattice antiferromagnet $NiGa_2S_4$ [3]. The complex magnetic and structural characteristics of low-dimensional spin systems make their magnetic state highly sensitive to external perturbations including temperature and magnetic field. For instance, the field-induced quantum phase transition from the Néel ordered phase to the spin liquid phase is observed in the quasi-1D antiferromagnet $BaCo_2V_2O_8$ [4], and a cascade of magnetization plateaus in the spin-chain system $Ca_3Co_2O_6$ [5–7].

Similar to other low-dimensional spin systems, the family of cobalt vanadium oxides $Co_xV_2O_{5+x}$ with $x = (1, 2, \text{or } 3)$ has also attracted special interest due to its low-dimensional characters in the aspect of magnetism [8–11]. For instance, it was found that the $x = 1$ compound CoV_2O_6 is a typical low-dimensional spin system, which crystallizes in two structural polymorphs with one having a monoclinic unit cell and the other having a triclinic unit cell [12], i.e., α-CoV_2O_6 and γ-CoV_2O_6. Although the two polymorphs possess different structural symmetries, both α-CoV_2O_6 and γ-CoV_2O_6 are quasi-1D Ising spin-chain compounds. An application of an external magnetic field leads to the observation of unusual 1/3 magnetization plateaus in both polymorphs [8,13–15], which is attributed to the strong spin exchange and the strong coupling between orbital, magnetic, and structural orders [16–18]. The $x = 3$ compound $Co_3V_2O_8$ exhibits a strong 2D

*liqinke@ameslab.gov
†zwouyang@mail.hust.edu.cn
‡y.xiao@pku.edu.cn

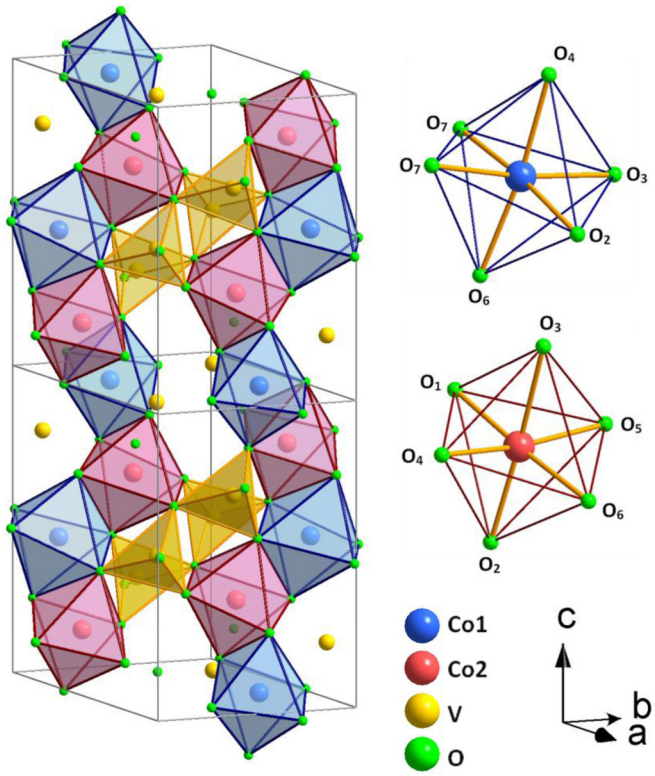

FIG. 1. The crystal structure of $Co_2V_2O_7$ at 300 K, which has the prototypical $K_2Cr_2O_7$-type structure with space group $P2_1/c$. The crystal structure can be described as the chains of edge-sharing CoO_6 octahedra with VO_4 tetrahedra in between. Two different types of CoO_6 octahedra, i.e., Co_1O_6 and Co_2O_6, are differentiated by color. The Co-O bond distances of Co_1O_6 and Co_2O_6 are illustrated for comparison.

magnetic character as it consists of buckled kagome layers with strong geometrical frustration [19,20]. Interestingly, a dielectric anomaly is observed around the ferromagnetic (FM) transition temperature indicating the existence of strong coupling between spin and charges in $Co_3V_2O_8$ [21].

As a member of the $Co_xV_2O_{5+x}$ family, the $x = 2$ compound $Co_2V_2O_7$ is considered as a chainlike low-dimensional spin compound. Structurally, $Co_2V_2O_7$ possesses two different Co^{2+} sites with two differing local bonding geometries, which are linked in a geometry that can be referred to as a zigzag chain consisting of arrays of edge-shared CoO_6 octahedra (see Fig. 1). The zigzag chains are interspersed with nonmagnetic V^{5+} ions in VO_4 pyramid blocks, resulting in a quasi-1D structural arrangement [10]. In a magnetic aspect, two fascinating magnetization plateaus—a 1/2-like plateau and a 3/4 plateau—are observed in $Co_2V_2O_7$, depending on crystallographic directions [22,23], which is quite different from the isostructural $Ni_2V_2O_7$ with a 1/2 plateau [24]. Given that the magnetization plateau is always observed in most of the chainlike low-dimensional systems with negligible interchain coupling, the observation of two plateaus also reflects that $Co_2V_2O_7$ belongs to a low-dimensional spin system.

In addition to applied magnetic fields, an applied electric field can also lead to novel magnetic states and unusual physical phenomena, such as multiferroicity, in low-dimensional spin systems. Indeed, magnetic-field-induced ferroelectricity was reported and found to be correlated with the magnetization plateaus in both $Co_2V_2O_7$ and $Ni_2V_2O_7$ [23]. Moreover, the deviations of the dielectric constant with respect to lattice contributions are evidently observed in $Co_2V_2O_7$ under zero magnetic field, suggesting the appearance of magnetostrictive effects induced by magnetic interactions [25]. To obtain further insight into the multiferroicity and spin-lattice couplings in the low-dimensional spin compound $Co_2V_2O_7$, we first investigate the magnetic ground state and nearby phases as well as the response of the lattice to the magnetic phase transitions.

Although there are a few reports on $Co_2V_2O_7$, its magnetic structure remains ambiguous, which is crucial to understand the field-induced magnetization plateaus, ferroelectricity, as well as the magnetostrictive effect. In this paper, we report on the structural and magnetic properties of $Co_2V_2O_7$ determined by magnetization and neutron powder diffraction methods. Both nuclear and magnetic structures are determined through a refinement of high-resolution neutron powder diffraction data at a low temperature of 2 K. It is found that $Co_2V_2O_7$ exhibits a noncollinear magnetic structure with Co spins forming a canted ↑↑↓↓ spin chain. The experimentally observed noncollinear magnetic ground state and electronic structure have also been examined and elucidated using *ab initio* calculations.

II. EXPERIMENTAL METHODS

A. Sample preparation and characterization

A polycrystalline sample of $Co_2V_2O_7$ was prepared using the sol-gel method by dissolving stoichiometric amounts of high-purity $Co(NO_3)_2 \cdot 6H_2O$ and NH_4VO_3 in deionized water. The x-ray powder diffraction measurement was carried out on a Huber diffractometer with Cu $K\alpha$ radiation $\lambda = 1.5406$ Å and a graphite monochromator. A Quantum Design Physical Property Measurement System (PPMS) was used to characterize the magnetic properties of the $Co_2V_2O_7$ powder sample in the temperature range from 2 to 350 K and a magnetic-field range from 0 to 9 T. The temperature dependence of magnetization was measured during warming from 2 to 350 K under 1000 Oe after cooling down from 350 K without the applied field [zero-field-cooled (ZFC)] or under the applied field [field-cooled (FC)], while the field dependence of magnetization was measured in magnetic fields up to 9 T at selective temperatures. By using a heat-capacity option of PPMS, the specific-heat measurements were also carried out on a small pellet of $Co_2V_2O_7$ sample with the thermal relaxation technique.

To study the crystal and magnetic structure of $Co_2V_2O_7$ systematically, time-of-flight (TOF) neutron powder diffraction (NPD) experiments were performed on the high-resolution neutron powder diffractometer POWGEN [26] at the Spallation Neutron Source (SNS) in Oak Ridge National Laboratory. About 5 g of the powder sample was loaded in an 8-mm-diameter vanadium sample holder and then installed in the helium cryostat that can reach low temperatures down to 2 K. Neutron diffraction data were collected for the $Co_2V_2O_7$ powder sample in the temperature range from 2 to 300 K. For

TABLE I. Refinement results of the crystal structure of $Co_2V_2O_7$ at 300 and 2 K. Both lattice parameters and the atomic positions for monoclinic space group $P2_1/c$ are listed.

Temperature		300 K				Temperature		2 K			
$a = 6.5932(2)$ Å		$b = 8.3775(2)$ Å		$c = 9.4782(2)$ Å		$a = 6.5860(2)$ Å		$b = 8.3681(2)$ Å		$c = 9.4635(2)$ Å	
$\alpha = 90°$		$\beta = 100.218(2)°$		$\gamma = 90°$		$\alpha = 90°$		$\beta = 100.191(2)°$		$\gamma = 90°$	
Type	Site	x	y	z	B_{iso}	Type	Site	x	y	z	B_{iso}
Co_1	4e	0.148(3)	0.123(3)	0.463(2)	0.45(2)	Co_1	4e	0.149(3)	0.121(3)	0.469(2)	0.24(1)
Co_2	4e	0.310(3)	0.382(3)	0.685(2)	0.45(2)	Co_2	4e	0.308(3)	0.389(3)	0.680(2)	0.24(1)
V_1	4e	0.34(2)	0.75(2)	0.53(2)	0.45(2)	V_1	4e	0.35(2)	0.75(2)	0.53(2)	0.24(1)
V_2	4e	0.19(2)	0.01(2)	0.81(2)	0.45(2)	V_2	4e	0.18(2)	0.01(2)	0.82(2)	0.24(1)
O_1	4e	0.604(1)	0.130(1)	0.123(1)	0.55(1)	O_1	4e	0.604(1)	0.130(1)	0.124(1)	0.19(1)
O_2	4e	0.428(1)	0.126(1)	0.396(1)	0.49(1)	O_2	4e	0.427(1)	0.127(1)	0.395(1)	0.07(1)
O_3	4e	0.170(1)	0.369(1)	0.461(1)	0.55(2)	O_3	4e	0.176(1)	0.370(1)	0.461(1)	0.16(1)
O_4	4e	0.255(1)	0.360(1)	0.183(1)	0.37(1)	O_4	4e	0.257(1)	0.359(1)	0.183(1)	0.04(1)
O_5	4e	0.678(1)	0.373(1)	0.347(1)	0.61(2)	O_5	4e	0.679(1)	0.373(1)	0.348(1)	0.19(1)
O_6	4e	0.028(1)	0.081(1)	0.246(1)	0.48(1)	O_6	4e	0.028(1)	0.083(1)	0.246(1)	0.12(1)
O_7	4e	0.852(1)	0.378(1)	0.006(1)	0.52(1)	O_7	4e	0.852(1)	0.379(1)	0.007(1)	0.21(1)
300 K, 1.066 Å		$R_p = 4.03$, $R_{wp} = 5.82$, $\chi = 0.50$				2 K, 1.066 Å		$R_p = 4.47$, $R_{wp} = 6.32$, $\chi = 0.58$			
300 K, 3.731 Å		$R_p = 3.72$, $R_{wp} = 5.35$, $\chi = 0.15$				2 K, 3.731 Å		$R_p = 5.39$, $R_{wp} = 8.46$, $\chi = 0.39$			

each temperature, the data were collected using two different center wavelengths, viz., 1.066 and 3.731 Å, to cover a large d-space range of 0.5–12 Å. The representation analyses were carried out using the program SARAH [27], whereas the crystal and magnetic structure refinements were carried out with the NPD data using the Rietveld refinement program FULLPROF Suite [28].

B. Calculation details

We have calculated the electronic structure, magnetic properties, and total energy differences between FM, AFM, and the experimental noncollinear (NC) magnetic states using the Vienna ab initio simulation package (VASP) [29,30]. The nuclei and core electrons were described by the projector augmented wave (PAW) potential [31]. The wave functions of valence electrons were expanded in a plane-wave basis set with a cutoff energy of up to 520 eV. The VASP calculations were performed with 240 k points in the IBZ. The correlation effects are also considered by using the generalized gradient approximation (GGA)+U method [32]. For transition metals, typical U values are between 1.5 and 6 eV [33]. Here, various U parameters between 0 and 4.8 eV are used to investigate the dependence of spin configuration on correlation effects. The experimental lattice parameters and atomic coordinates measured through neutron diffraction at 2 K, as listed in Table I, were used in all the calculations.

III. EXPERIMENTAL RESULTS AND DISCUSSION

A. Magnetization and magnetic phase transition

Figure 2(a) shows the temperature dependence of the magnetization of the $Co_2V_2O_7$ polycrystalline sample under magnetic fields of 1000 Oe. With decreasing temperature, the magnetization increases smoothly in the temperature range from 350 K to around 6 K, while it starts decreasing when the sample is cooled further. The phase transition at around 6 K can be clearly observed as indicated by the anomalies in magnetization data measured in both zero-field-cooling and field-cooling modes. To deduce the magnetic phase transition temperature precisely, the measurement on the temperature dependence of the specific heat is performed under zero magnetic field as shown in Fig. 2(b), in which a clear phase transition is detected at 6.0(2) K. The transition temperature of 6.0 K can be denoted as the Néel temperature T_N where the paramagnetic state develops from the antiferromagnetic phase with increasing temperature, as will be demonstrated by neutron diffraction results in the following text.

The temperature dependence of the inverse susceptibility $1/\chi$ of the $Co_2V_2O_7$ compound is also exhibited in Fig. 2(a). It is known that the magnetic susceptibility of localized noninteracting magnetic ions in the high-temperature region can be written as $\chi(T) = \frac{C}{T-\Theta_{CW}}$, where C and θ_{CW} are the Curie constant and Curie-Weiss (CW) temperature, respectively. The Curie constant can be expressed as $C = NM_{eff}^2\mu_B^2/3k_B$, where N is the density of magnetic ions, M_{eff} is the effective paramagnetic moment, k_B is the Boltzmann constant, and μ_B is the Bohr magneton [34]. As indicated in Fig. 2(a), the susceptibility strictly follows the Curie-Weiss behavior in the high-temperature range, while the inverse susceptibility $1/\chi$ deviated from the Curie-Weiss estimation below 120 K, indicating the onset of considerable magnetic correlations. The effective paramagnetic moment is deduced to be $3.77(1)\mu_B$ and it matches very well with the effective magnetic moment of Co^{2+}, which can be obtained using $p_{eff} = g\sqrt{S(S+1)}$, where $g = 2$ is the Landé g factor and $S = 3/2$. The fit of high-temperature susceptibility by means of the Curie-Weiss law gives a negative Curie-Weiss temperature of $-16.1(5)$ K, indicating that the dominant magnetic interactions are antiferromagnetic in $Co_2V_2O_7$. Moreover, by comparing the Curie-Weiss temperature θ_{CW} with the Néel temperature T_N, the frustration parameter [35] $f = |\Theta_{CW}|/T_N$ is obtained to be 2.5(1), suggesting a moderate spin frustration in $Co_2V_2O_7$.

Figure 3(a) shows magnetization measured as a function of magnetic field at 2 K. Although the magnetization increases monotonically upon the application of the magnetic field,

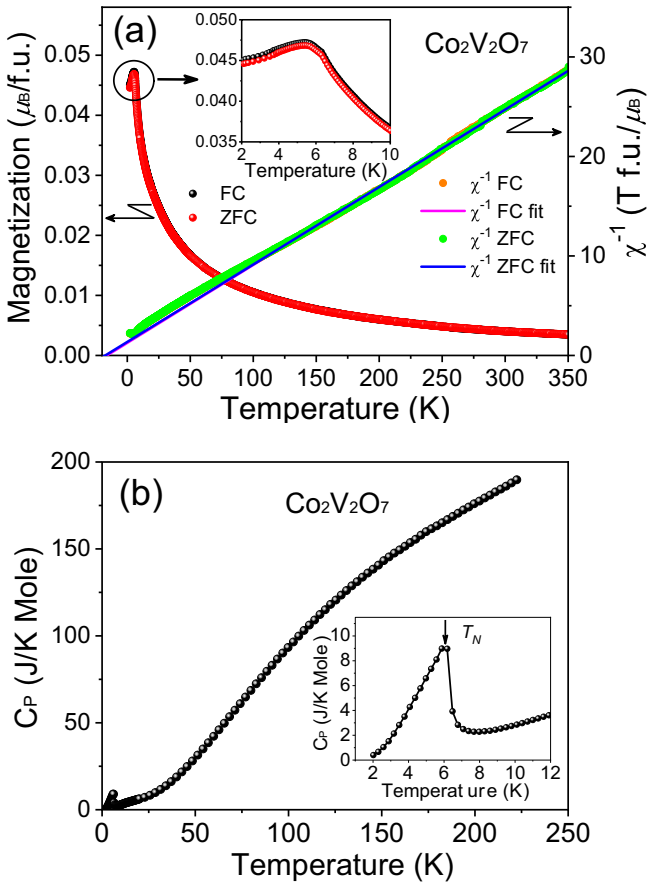

FIG. 2. (a) Temperature dependence of the magnetization and inverse magnetic susceptibility χ^{-1} of $Co_2V_2O_7$ measured in zero-field-cooling and field-cooling modes under a magnetic field of 1000 Oe. The inset of (a) shows an enlarged view of the magnetization in the low-temperature region. Solid lines indicate Curie-Weiss fits to inverse susceptibility in the high-temperature region from 200 to 350 K as described in the text. (b) The temperature dependence of specific heat *Cp* of $Co_2V_2O_7$. The inset of (b) shows an enlarged view of the *Cp* in the low-temperature region.

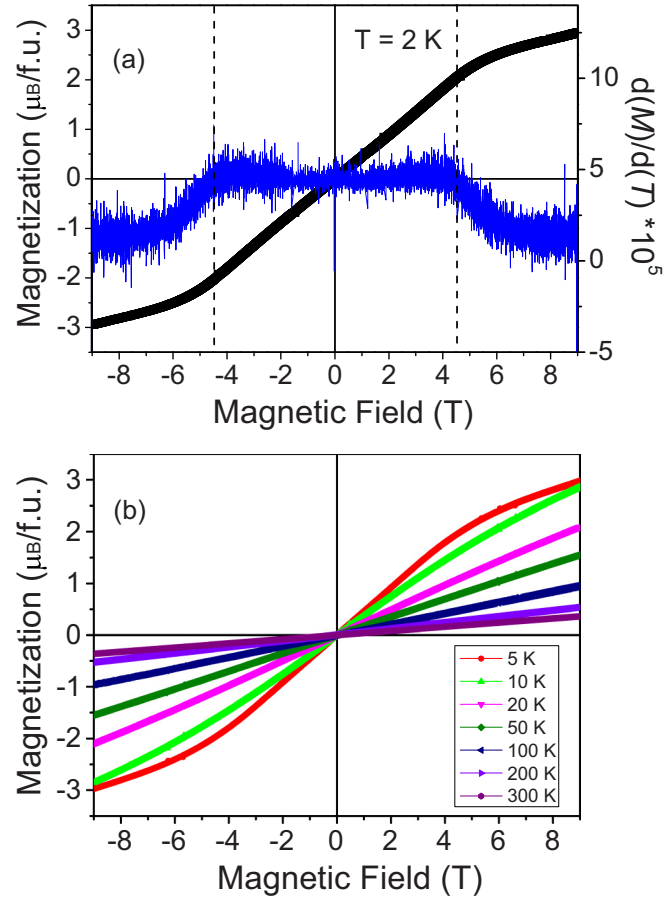

FIG. 3. (a) Magnetization as a function of magnetic field for $Co_2V_2O_7$ at 2 K. The dashed line indicates the field-induced spin-flop transition at 4.2 T as determined from the anomaly in the derivative curve of the magnetization. (b) Magnetic-field dependence of the magnetization of $Co_2V_2O_7$ measured at different temperatures between 5 and 300 K.

the saturated magnetization still could not be reached upon the application of the magnetic field up to 9 T. It is also noticed that a kink takes place at 4.2 T in the *M-H* curve, which suggests that $Co_2V_2O_7$ undergoes a spin-flop transition with increasing magnetic field. The field-induced spin-flop transition is also clearly emphasized in the derivative curve of the magnetization data, and it can be considered as the result of the competition between Zeeman energy $E = -\mu_0 \vec{M} \cdot \vec{H}$ and magnetic anisotropy energy in $Co_2V_2O_7$. The *M-H* curves at various temperatures are presented in Fig. 3(b). The spin-flop transition can still be observed at 5 K, while it is not discernible once temperature increased to above T_N. Nevertheless, a considerable magnetization value, e.g., 2.85μ_B/f.u. at 10 K and 9 T, can still be obtained above T_N, which indicates that the application of a magnetic field can not only change the ordering configuration but also enhances the magnetic ordering temperature of the Co^{2+} moment. With a further increase in temperature, the magnetization of $Co_2V_2O_7$ decreased and exhibited typical antiferromagnetic behavior.

B. Crystal structure and noncollinear magnetic ground state determined by NPD

To clarify the magnetic ground state of $Co_2V_2O_7$, neutron diffraction patterns were collected in a wide temperature range from 2 to 300 K. Figure 4 shows the NPD patterns of $Co_2V_2O_7$ at 300 and 2 K. Two different center wavelengths, i.e., 1.066 and 3.731 Å, are applied during the measurements so that a great number of diffraction peaks can be obtained in a large *d*-space from 0.5 to 12 Å. Two neutron diffraction patterns collected with two different center wavelengths were simultaneously refined for each temperature. At 300 K, $Co_2V_2O_7$ crystallizes in the monoclinic phase with space group $P2_1/c$. By taking advantage of the large neutron scattering cross section of oxygen, the accurate position of oxygen atoms can be easily determined. However, the atomic position of vanadium cannot be determined precisely as the nuclei of vanadium have a small coherent neutron scattering cross section. Therefore, x-ray diffraction patterns are collected for $Co_2V_2O_7$ at 300 K to determine the atomic position of vanadium since vanadium is a strong scatterer of x rays. The detailed structural information for $Co_2V_2O_7$ at 300 K, as obtained from combining refinement of both NPD and XRD data, is given in Table I.

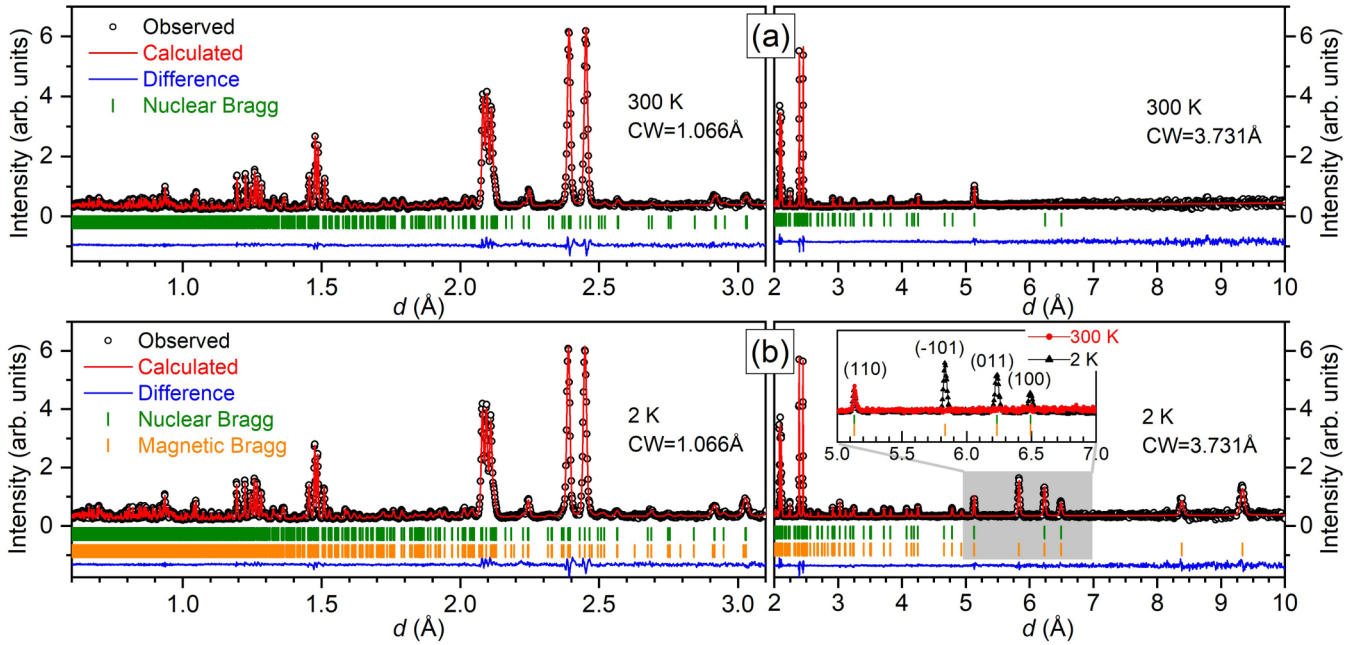

FIG. 4. Rietveld refinement results of neutron powder diffraction patterns for $Co_2V_2O_7$ at (a) 300 K and (b) 2 K. The left and right panels show the data collected at the center-wavelength (CW) 1.066 and 3.731 Å, respectively. The patterns in (b) are refinement results obtained by adopting a magnetic structure model with irreducible representation Γ_2 as described in the text. The circles represent the observed intensity, and the solid line is the calculated pattern. The difference between the observed and calculated intensities is shown at the bottom. The vertical bars indicate the expected nuclear and magnetic Bragg reflection positions. The inset shows a part of the diffraction pattern for 2 and 300 K data indicating the additional magnetic reflections upon cooling.

The crystal structure of $Co_2V_2O_7$ and the octahedra of CoO_6 are illustrated in Fig. 1. The bond lengths and bond angles of CoO_6 octahedra at 300 K are shown in Table II. The average Co-O bond lengths of CoO_6 for two nonequivalent Co sites, Co_1 and Co_2, are 2.074(5) and 2.083(5) Å, respectively, indicating a slightly different degree of distortion for these two octahedra. With decreasing temperature, the monoclinic structure of $Co_2V_2O_7$ persists down to 2 K accompanied by a shrinkage of lattice. The results of structural refinements at 2 K are also presented in Table I.

In contrast to the NPD patterns at 300 K, extra peaks with considerable intensities show up once the sample was cooled to 2 K, which is below the Néel temperature $T_N = 6.0$ K. Most of the new emerging peaks possess relatively large d-values and can be assigned as magnetic Bragg peaks, indicating the formation of long-range magnetic order of Co^{2+} moments. It is also found that all magnetic reflections can be indexed as commensurate reflections with the magnetic propagation wave vector $\mathbf{k} = (0, 0, 0)$, which means that the magnetic structure is commensurate in nature.

TABLE II. The bond length and bond angle of CoO_6 octahedra in $Co_2V_2O_7$ at 300 K.

Co_1	300 K	Co_2	300 K
O_2	2.0521 Å	O_1	2.1298 Å
O_3	2.0675 Å	O_2	2.0105 Å
O_4	2.0878 Å	O_3	2.1642 Å
O_6	2.0956 Å	O_4	2.0663 Å
O_7	2.0649 Å	O_5	2.0677 Å
O_7	2.0746 Å	O_6	2.0592 Å
O_2-Co_1-O_3	85.16°	O_1-Co_2-O_4	96.40°
O_2-Co_1-O_7	94.63°	O_1-Co_2-O_5	87.08°
O_3-Co_1-O_7	94.65°	O_4-Co_2-O_6	88.93°
O_7-Co_1-O_7	86.44°	O_5-Co_2-O_6	87.67°
O_4-Co_1-O_6	173.43°	O_2-Co_2-O_3	174.35°
Average Co-O bond length			
300 K	Co_1-O = 2.0737	Co_2-O = 2.0829	

Symmetry analysis allows the determination of the symmetry-allowed magnetic structures based on the representation theory. Magnetic symmetry analysis was carried out for $Co_2V_2O_7$ using the program SARAH [27] by which the allowed symmetry couplings in the form of irreducible representation and their basis vectors can be deduced. It is known that two Co^{2+} ions occupy two inequivalent crystallographic Wyckoff sites $2e$ in $Co_2V_2O_7$ with the crystallographic space group $P2_1/c$. With the commensurate magnetic propagation vector $\mathbf{k} = (0, 0, 0)$, both Co ions are found to have four one-dimensional irreducible magnetic representations (IRs), i.e., Γ_1, Γ_2, Γ_3, and Γ_4, and each of them is composed of three basis vectors (BVs) with only real components. Assuming that Co atoms located at two nonequivalent crystallographic sites carry magnetic moments with different amplitude as in the $Co_3V_2O_8$ [19] counterpart, all possible IRs are adopted into the magnetic structural model and used to fit against the NPD pattern at 2 K.

As demonstrated in Fig. 4(b) (right panel), a satisfactory fitting of all magnetic reflections can only be obtained by using IR Γ_2 with a Shubnikov space group of $P2_1/c'$, while the other three representations can be ruled out due to poor fit of magnetic reflections. The decomposition of the magnetic

TABLE III. Nonzero basis vectors (BVs) of the irreducible representations (IRs) and positional coordinates for Co atoms that were used to describe the noncollinear magnetic structure of $Co_2V_2O_7$ with space group $P2_1/c$ and propagation vector $k = (0, 0, 0)$.

			BV components			Positional coordinates		
IR	BV	Atom	$m_{\|\|a}$	$m_{\|\|b}$	$m_{\|\|c}$	x	y	z
Γ_2	ψ_4	1	1	0	0	x	y	z
		2	−1	0	0	$\bar{x}+1$	$y+\frac{1}{2}$	$\bar{z}+\frac{1}{2}$
		3	−1	0	0	$\bar{x}+1$	$\bar{y}+1$	$\bar{z}+1$
		4	1	0	0	x	$\bar{y}+\frac{1}{2}$	$z+\frac{1}{2}$
	ψ_5	1	0	1	0	x	y	z
		2	0	1	0	$\bar{x}+1$	$y+\frac{1}{2}$	$\bar{z}+\frac{1}{2}$
		3	0	−1	0	$\bar{x}+1$	$\bar{y}+1$	$\bar{z}+1$
		4	0	−1	0	x	$\bar{y}+\frac{1}{2}$	$z+\frac{1}{2}$
	ψ_6	1	0	0	1	x	y	z
		2	0	0	−1	$\bar{x}+1$	$y+\frac{1}{2}$	$\bar{z}+\frac{1}{2}$
		3	0	0	−1	$\bar{x}+1$	$\bar{y}+1$	$\bar{z}+1$
		4	0	0	1	x	$\bar{y}+\frac{1}{2}$	$z+\frac{1}{2}$

representation Γ_2 in terms of basis vectors is given in Table III. According to Γ_2, the Co moments align antiferromagnetically in the magnetic unit cell and the refined vector components of the magnetic moment are obtained to be different for two individual Co $2e$ sites, i.e., $m_x = -0.26(5)\mu_B$, $m_y = 1.77(5)\mu_B$, and $m_z = 0.97(5)\mu_B$ for the Co_1 site, and $m_x = 0.35(5)\mu_B$, $m_y = 2.38(5)\mu_B$, and $m_z = 1.27(5)\mu_B$ for the Co_2 site, respectively. It is obvious that the canted Co moments ordered antiferromagnetically in almost the b-c plane and form a spin-chain-like structure along the c-axis, as illustrated in Fig. 5.

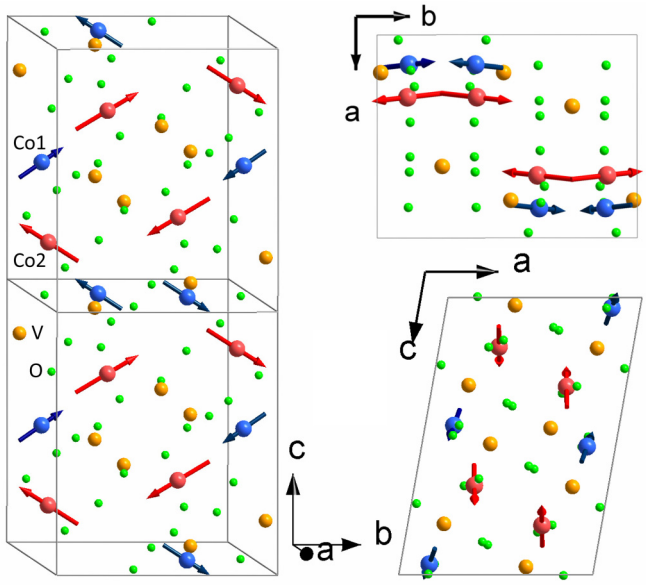

FIG. 5. Illustration of the noncollinear magnetic structure of $Co_2V_2O_7$ below the magnetic transition temperature. The Co moments ordered antiferromagnetically in almost the b-c plane. The magnetic unit cell is identical to the monoclinic structural unit cell, which is outlined with the gray lines.

The refined magnetic moments of Co in the spin chain are 2.06 (5) and 2.69 (5) μ_B for Co_1 and Co_2, respectively. The canted angle of the Co moment toward the c-axis is around 26(3)°. Nevertheless, the tilt of Co spin does not follow the tilt of CoO_6 octahedra, suggesting the negligible influence of the electric multipolar field generated by oxygen neighbors on the orbitals of Co ions. The antiferromagnetic ground state of $Co_2V_2O_7$ is apparently determined by the interplay between spin-spin exchange interaction and magnetocrystalline anisotropy, which are largely dependent on the electronic configuration of Co ions. It is known that the up-up-down-down spin arrangement along the alternating array of two magnetic sites might break the inversion symmetry, and the inequivalent exchange striction working between the up-up (or down-down) spin pair and the up-down (or down-up) spin pair can produce electric polarization along the chain direction [36]. The exchange-striction mechanism might be applied to $Co_2V_2O_7$ with canted ↑↑↓↓ spin chains (see Fig. 5), and the electric polarization will emerge as a consequence.

C. Calculation results on a magnetic ground state

The calculation started with the experimental spin structure to investigate the electronic structure and magnetic properties of $Co_2V_2O_7$. Two sets of noncollinear calculations are performed: One was with a constraint that fixes Co magnetic moment directions during self-consistent calculations, and the other was without this constraint so that both the directions and magnitudes of each Co magnetic moment were relaxed. Table IV shows the magnetic moment components of each Co atom obtained from NC magnetic calculations with and without relaxing the spin directions. Experimental values are also included for comparison. The calculations were carried out using DFT+U with $U = 3.2$ eV. The calculations show similar magnetic moments for two nonequivalent Co sites while the experiment found noticeably different magnetic moments between two Co sites. The further relaxation of spin direction only introduces small changes on the amplitudes and directions of Co moments, suggesting the obtained spin structure is rather stable.

Atom-projected partial densities of states (PDOS) of the relaxed spin configuration are shown in Fig. 6. The calculations were performed within GGA and GGA+U with $U = 3.2$ eV, respectively. In the case of $U = 0$ eV, there are sharp Co-DOS peaks near the Fermi energy. The band gap sits between two sharp DOS peaks, which mostly consist of Co d states that barely hybridize with other states and form flat bands. The band gap is about 0.25 eV within GGA and depends on the applied U parameters with GGA+U. The PDOS with $U = 3.2$ eV are shown in Fig. 6(b). As expected, a larger band gap is obtained. It seems that the U potential is able to rearrange Co states to promote the hybridization of Co d states with other states so that NC magnetic structure becomes stable. It would be interesting to measure the band gap, which may guide justifying the U parameter.

Considering that the relaxed spin configuration is potentially a metastable spin configuration, here we calculate and compare the total energies of FM, AFM, and NC magnetic structures using VASP. The dependence of these energy differences on the correlation parameter U is also investigated. The plain DFT calculations show that the FM state has the

TABLE IV. Comparison of measured and calculated magnetic moments of two Co sites in $Co_2V_2O_7$. The Co magnetic moments are in units of μ_B.

	Experiment			Constrained			Relaxed		
	m_x	m_y	m_z	m_x	m_y	m_z	m_x	m_y	m_z
Co_1	−0.260	1.773	0.968	−0.34	2.32	1.27	−0.30	2.33	1.25
	0.260	1.773	−0.968	0.34	2.32	−1.27	0.30	2.33	−1.25
	0.260	−1.773	−0.968	0.34	−2.32	−1.27	0.29	−2.34	−1.25
	−0.260	−1.773	0.968	−0.34	−2.32	1.27	−0.30	−2.34	1.24
Co_2	0.348	2.376	1.271	0.34	2.33	1.24	0.37	2.37	1.15
	−0.348	−2.376	−1.271	−0.34	−2.33	−1.24	−0.37	−2.38	−1.14
	−0.348	2.376	−1.271	−0.34	2.33	−1.24	−0.36	2.37	−1.15
	0.348	−2.376	1.271	0.34	−2.33	1.24	0.37	−2.37	1.15

lowest energy, which is 3.86 and 19.88 eV/Co lower than the AFM state and the NC state, respectively. In general, the DFT+U method gives better agreement with experimental results than the plain DFT method for oxide gap materials because of strong correlation. We performed calculations with three different U parameters to understand their effects on the magnetic states. Table V shows the total energies for FM, AFM, and NC magnetic structures with various U values. It shows that the magnetic ground state depends on the magnitude of the U potential. A larger U parameter tends to stabilize the NC state.

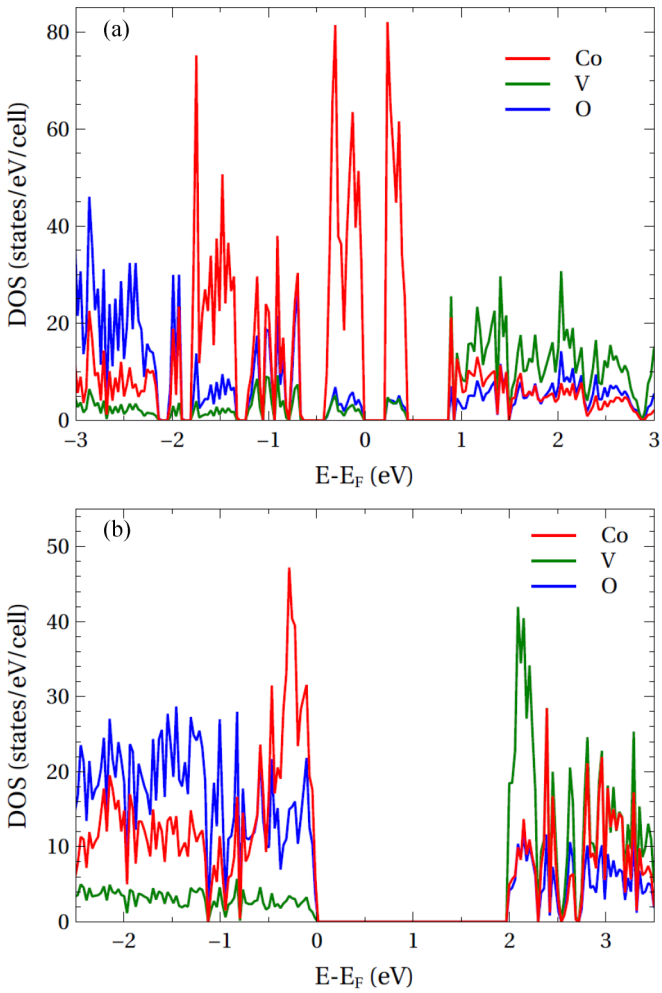

FIG. 6. Atom-projected partial densities of states of the NC magnetic structure. They are calculated within (a) GGA and (b) GGA+U with $U = 3.2$ eV.

D. Anisotropic magnetoelastic coupling and thermal expansion

The change of individual lattice parameters with temperature can be obtained through the refinement of NPD patterns collected at different temperatures. As shown in Figs. 7(a)–7(d), the onset of magnetoelastic distortions below $T_N = 6.0$ K is clearly visible for lattice parameters a and b, while the lattice parameters c and β stay almost constant upon crossing the Néel temperature. It is worth noting that the sign of the deviation for a is opposite to that for b, indicating the existence of anisotropic magnetoelastic coupling in $Co_2V_2O_7$. The corresponding unit-cell volume is shown in Fig. 7(e). Although a elongates and b shrinks upon cooling below T_N, they compensate each other in the volumetric expansion. The unit-cell volume V shows no anomalous change and increases monotonically with temperature.

Because the tilt of Co spin does not follow the tilt of CoO_6 octahedra, we speculate that the influence of the electric multipolar field generated by oxygen neighbors on the orbitals of Co ions is negligible. The antiferromagnetic ground state of $Co_2V_2O_7$ is apparently determined by the interplay between spin-spin exchange interaction and single-ion anisotropy. To understand anisotropic magnetoelastic coupling and thermal expansion, we correlate the variation of distance between different Co ions in the same spin-chain along the c-axis to

TABLE V. Calculated total energy (meV/Co) of FM, AFM, and experimental noncollinear (denoted as NC) magnetic states with $U = 0$, 1.6, 3.2, and 4.8 eV using VASP. Calculated band-gap range (E_{gap}) is given in the bottom row. While band-gap is more or less similar for different spin configurations, it depends on U parameter.

U (eV)	0	1.6	3.2	4.8
E_{FM}	0.00	0.00	0.00	0.00
E_{AFM}	3.86	−8.59	20.78	18.72
E_{NC}	19.88	−7.17	−5.06	−3.18
E_{gap}	0.23–0.25	1.26–1.37	1.86–1.99	2.14–2.28

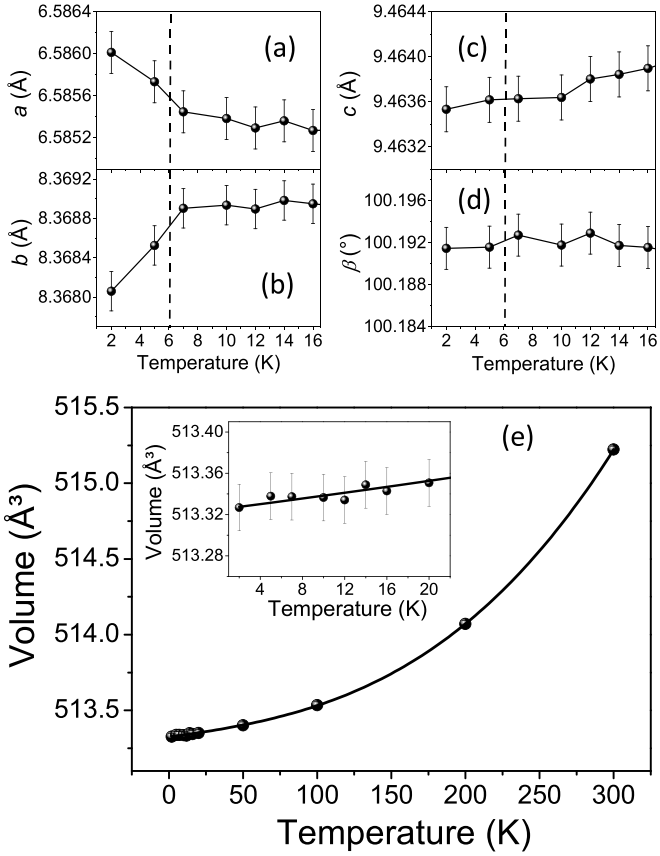

FIG. 7. (a)–(d) Temperature dependence of the estimated lattice parameters a, b, c, and β. (e) Temperature dependence of the unit-cell volume of $Co_2V_2O_7$. The inset shows the variation of the unit-cell volume in the low-temperature range.

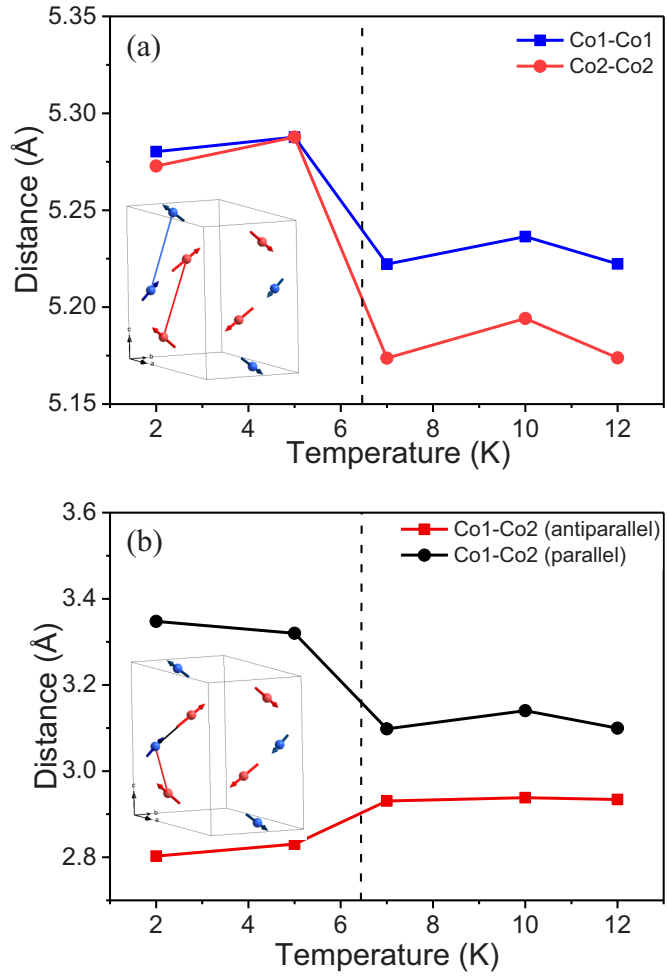

FIG. 8. Temperature dependence of the change of distance between different Co ions in same spin chain along the c-axis. The insets illustrate the Co-Co pairs in the unit cell of $Co_2V_2O_7$.

the antiferromagnetic phase transition. The change of distance between neighboring Co sites at different temperatures is shown in Fig. 8(a). Both of the distances of Co_1-Co_1 and Co_2-Co_2 decrease with the increasing of temperature and remain almost constant above T_N. Figure 8(b) displays the temperature dependence of the change of distance between different Co sites. According to the noncollinear magnetic structure illustrated in Fig. 5, two nonequivalent Co sites in the same spin-chain form parallel or antiparallel spin configurations. The distance of Co_1-Co_2 with parallel spin ordering shows the same behavior as the lattice parameter b, and the distance of Co_1-Co_2 with antiparallel spin ordering shows the same behavior as the lattice parameter a. This is clear evidence that the anisotropic magnetoelastic coupling and thermal expansion of lattice parameters are most likely associated with the different exchange interactions between two neighboring Co spins.

IV. CONCLUSIONS

In summary, we have studied the magnetic properties of $Co_2V_2O_7$ via extensive approaches, such as magnetization measurements, neutron powder diffraction measurements, and theoretical calculations. By modeling the temperature dependence of the magnetization with the Curie-Weiss law, we find that the Curie-Weiss temperature is negative, e.g., $-16.1(5)$ K, indicating dominating antiferromagnetic coupling. A spin-flop transition was observed while the magnetic field was applied below $T_N = 6.0$ K. By applying neutron powder diffraction methods, we confirm that $Co_2V_2O_7$ remains monoclinic from 300 K down to 2 K. The magnetic ground state was determined unambiguously based on NPD results by using representation analysis combined with magnetic Rietveld refinements. Two nonequivalent Co sites with different magnetic moments form a spin-chain-like structure along the c-axis and canted antiferromagnetic ordering in almost the b-c plane. By comparing total energies between different magnetic states, we found that the theoretical magnetic ground state is sensitive to the U parameter and GGA+U calculations show that the noncollinear magnetic state possesses a lower energy than FM and AFM states. The ferroelectricity in $Co_2V_2O_7$ might be understood based on the exchange striction model, which can be applied to canted ↑↑↓↓ spin configurations. Moreover, the temperature dependence of lattice parameters in $Co_2V_2O_7$ exhibits an anisotropic magnetoelastic coupling between the a, b, and c below T_N.

ACKNOWLEDGMENTS

This work was supported by the National Natural Science Foundation of China (Grant No. 11874023) and Project Based Personnel Exchange Program (PPP) with China Scholarship Council (CSC Nos. 2016-6041) and German Academic Exchange Service (Project-ID 57219934). Part of the research conducted at SNS was sponsored by the Scientific User Facilities Division, Office of Basic Energy Sciences, U.S. Department of Energy. W.H.J. would like to acknowledge financial support from the China Scholarship Council (CSC). The research at the University of Macau was supported by SRG2016-00091-FST and the Science and Technology Development Fund, Macau SAR (File no. 063/2016/A2, File no. 064/2016/A2, File no. 028/2017/A1, and File no. 0051/2019/AFJ). Work at Ames Laboratory was supported by the U.S. Department of Energy, Basic Energy Sciences, Materials Sciences and Engineering Division, and the Office of Science Early Career Research Program. Ames Laboratory is operated for the U.S. Department of Energy by Iowa State University under Contract No. DE-AC02-07CH11358. This research used resources of the National Energy Research Scientific Computing Center (NERSC), a U.S. Department of Energy Office of Science User Facility operated under Contract No. DE-AC02-05CH11231.

[1] D. A. Tennant, T. G. Perring, R. A. Cowley, and S. E. Nagler, Phys. Rev. Lett. **70**, 4003 (1993).

[2] B. Lake, D. A. Tennant, C. D. Frost, and S. E. Nagler, Nat. Mater. **4**, 329 (2005).

[3] S. Nakatsuji, Y. Nambu, H. Tonomura, O. Sakai, S. Jonas, C. Broholm, H. Tsunetsugu, Y. Qiu, and Y. Maeno, Science **309**, 1697 (2005).

[4] S. Kimura, H. Yashiro, K. Okunishi, M. Hagiwara, Z. He, K. Kindo, T. Taniyama, and M. Itoh, Phys. Rev. Lett. **99**, 087602 (2007).

[5] P. Lampen, N. S. Bingham, M. H. Phan, H. Srikanth, H. T. Yi, and S. W. Cheong, Phys. Rev. B **89**, 144414 (2014).

[6] H. Kageyama, K. Yoshimura, K. Kosuge, H. Mitamura, and T. Goto, J. Phys. Soc. Jpn. **66**, 1607 (1997).

[7] Y. B. Kudasov, Phys. Rev. Lett. **96**, 027212 (2006).

[8] Z. He, J.-I. Yamaura, Y. Ueda, and W. Cheng, J. Am. Chem. Soc. **131**, 7554 (2009).

[9] Y. Drees, S. Agrestini, O. Zaharko, and A. C. Komarek, Cryst. Growth Design **15**, 1168 (2015).

[10] Z. He, J.-I. Yamaura, Y. Ueda, and W. Cheng, J. Solid State Chem. **182**, 2526 (2009).

[11] G. Balakrishnan, O. A. Petrenko, M. R. Lees, and D. Mc. K. Paul, J. Phys.: Condens. Matter **16**, L347 (2004).

[12] K. Mocala and J. Ziolkowski, J. Solid State Chem. **69**, 299 (1987).

[13] M. Lenertz, J. Alaria, D. Stoeffler, S. Colis, and A. Dinia, J. Phys. Chem. C **115**, 17190 (2011).

[14] M. Nandi and P. Mandal, J. Appl. Phys. **119**, 133904 (2016).

[15] H. Shu, Z. Ouyang, Y. Sun, M. Ruan, J. Li, X. Yue, Z. Wang, Z. Xia, and G. Rao, J. Magn. Magn. Mater. **407**, 129 (2016).

[16] F. Wallington, A. M. Arevalo-Lopez, J. W. Taylor, J. R. Stewart, V. Garcia-Sakai, J. P. Attfield, and C. Stock, Phys. Rev. B **92**, 125116 (2015).

[17] N. Hollmann, S. Agrestini, Z. Hu, Z. He, M. Schmidt, C. Y. Kuo, M. Rotter, A. A. Nugroho, V. Sessi, A. Tanaka, N. B. Brookes, and L. H. Tjeng, Phys. Rev. B **89**, 201101(R) (2014).

[18] S. A. J. Kimber, H. Mutka, T. Chatterji, T. Hofmann, P. F. Henry, H. N. Bordallo, D. N. Argyriou, and J. P. Attfield, Phys. Rev. B **84**, 104425 (2011).

[19] Y. Chen, J. W. Lynn, Q. Huang, F. M. Woodward, T. Yildirim, G. Lawes, A. P. Ramirez, N. Rogado, R. J. Cava, A. Aharony *et al.*, Phys. Rev. B **74**, 014430 (2006).

[20] M. Ramazanoglu, C. P. Adams, J. P. Clancy, A. J. Berlinsky, Z. Yamani, R. Szymczak, H. Szymczak, J. Fink-Finowicki, and B. D. Gaulin, Phys. Rev. B **79**, 024417 (2009).

[21] N. Bellido, C. Martin, C. Simon, and A. Maignan, J. Phys.: Condens. Matter **19**, 056001 (2007).

[22] L. Yin, Z. W. Ouyang, J. F. Wang, X. Y. Yue, R. Chen, Z. Z. He, Z. X. Wang, Z. C. Xia, and Y. Liu, Phys. Rev. B **99**, 134434 (2019).

[23] R. Chen, J. F. Wang, Z. W. Ouyang, Z. Z. He, S. M. Wang, L. Lin, J. M. Liu, C. L. Lu, Y. Liu, C. Dong *et al.*, Phys. Rev. B **98**, 184404 (2018).

[24] Z. W. Ouyang, Y. C. Sun, J. F. Wang, X. Y. Yue, R. Chen, Z. X. Wang, Z. Z. He, Z. C. Xia, Y. Liu, and G. H. Rao, Phys. Rev. B **97**, 144406 (2018).

[25] M. Sanchez-Andujar, S. Yanez-Vilar, J. Mira, N. Biskup, J. Rivas, S. Castro-Garcia, and M. A. Senaris-Rodriguez, J. Appl. Phys. **109**, 054106 (2011).

[26] A. Huq, J. P. Hodges, O. Gourdon, and L. Heroux, Z. Krist. Proc. **1**, 127 (2011).

[27] A. Wills, Physica B **276**, 680 (2000).

[28] J. Rodríguez-Carvajal, Physica B **192**, 55 (1993).

[29] G. Kresse and J. Hafner, Phys. Rev. B **47**, 558 (1993).

[30] G. Kresse and J. Furthmuller, Phys. Rev. B **54**, 11169 (1996).

[31] G. Kresse and D. Joubert, Phys. Rev. B **59**, 1758 (1999).

[32] S. L. Dudarev, G. A. Botton, S. Y. Savrasov, C. Y. Humphreys, and A. P. Sutton, Phys. Rev. B **57**, 1505 (1998).

[33] E. Şaşıoğlu, C. Friedrich, and S. Blügel, Phys. Rev. B **83**, 121101(R) (2011).

[34] H.-F. Li, A. Wildes, B. Hou, C. Zhang, B. Schmitz, P. Meuffels, G. Roth, and T. Brückel, RSC Adv. **4**, 53602 (2014).

[35] L. Balents, Nature (London) **464**, 199 (2010).

[36] Y. Tokura, S. Seki, and N. Nagaosa, Rep. Progr. Phys. **77**, 076501 (2014).